Atmospheric
Measurement
Techniques
Discussions

Performance of SIFT-MS and PTR-MS in the measurement of volatile organic compounds at different humidities

Ann-Sophie Lehnert[1,2], Thomas Behrendt[1], Alexander Ruecker[1], Georg Pohnert[2], Susan E. Trumbore[1]

5

[1]Department of Biogeochemical Processes, Max Planck Institute for Biogeochemistry, 07745 Jena, Germany
[2]Institute for Inorganic and Analytical Chemistry, Friedrich Schiller University, 07743 Jena, Germany

10

Correspondence to:

Ann-Sophie Lehnert (alehnert@bgc-jena.mpg.de)

15   Department of Biogeochemical Processes

Max Planck Institute for Biogeochemistry

Hans-Knoell-Straße 10, 07743 Jena, Germany

20

25

Abstract. As direct real-time analysis techniques, Selective Ion Flow Tube Mass Spectrometry (SIFT-MS) and Proton-Transfer Reaction Mass Spectrometry (PTR-MS) provide on-line measurement of volatile organic compounds (VOCs). Both techniques are widely-used across several disciplines, *e.g.* atmospheric chemistry, food science and medicine. However, the humidity of the sampled air greatly influences the quantified mixing ratio, and must be accounted for in the calibration of both platforms. Here we present both an evaluation of calibration functions taking account for humidity and a "side-by-side" comparison of the performance of the two instruments based upon a calibration of 15 different VOCs over a relative humidity range from 0-90 % at 25° C. While we made several improvements to a Voice 200 ultra SIFT-MS instrument to reduce background levels, overall detection limits for a PTR-QMS 500 are an order of magnitude lower. Sensitivity (here defined as the slope of the calibration curve) was higher for the SIFT-MS, and its calibration was more robust against humidity compared to PTR-MS. Thus, PTR-MS is the method of choice for simple, low-concentration, low-humidity analyses with a limited number of compounds whereas SIFT-MS is better-suited for more complex systems with varying humidity like our experiments investigating the change in VOC emissions of soils during dryout.

1   Introduction

Volatile organic compounds (VOCs) shape the medium we are living in: the air. As odours, pheromones, reductants, greenhouse gases and precursors for aerosols, they regulate key processes in the environment. Due to their reactivity, their atmospheric lifetimes are usually limited, and their mixing ratios are rather low and span several orders of magnitude, typically tens of parts per trillion (ppt) – low parts per million (ppm). Despite great improvements during the past years, methods of measuring VOC that rely on concentrating samples using adsorption tubes, or trapping air in storage containers often have artefacts due to dissipation of the analytes to, or reactions with, the walls or sorptive materials (Piennar *et al.*, 2015, Herrington, 2015).

Thus, an easy, fast, and direct analysis method is desirable. Proton-Transfer Reaction Mass Spectrometry (PTR-MS) and Selective Ion Flow Tube Mass Spectrometry (SIFT-MS) both provide these characteristics as they do not rely on time-consuming sample separation like Gas Chromatography/Mass Spectrometry. Both are used in a wide variety of fields comprising both natural and anthropogenic atmospheric chemistry (Milligan *et al.*, 2002; Yuan *et al.*, 2017), plant studies (Amelynck *et al.*, 2013), food science (Davis *et al.*, 2005), and medical applications like breath-analysis (Schwarz *et al.*, 2009; Shende *et al.*, 2017; Smith *et al.*, 2014).

The two techniques have been compared in various reviews, *e.g.* Bylinski, *et al.* (2017), Casas-Ferreira *et al.* (2019), Smith and Spanel (2011), and therefore, main differences between SIFT-MS and PTR-MS are only discussed briefly here. The principle behind both instruments is the chemical ionization of the analyte during a defined reaction time. Thus, the amount of compound can be calculated from the number of detected product ions using the kinetic rate constants k of the ionization reaction of the analyte A with the reagent ion R^+:

$$A + R^+ \rightarrow A^+ + R \tag{R1}$$

$$\frac{d[R]}{dt} = k \cdot [A] \cdot [R^+] \tag{1}$$

Assuming a pseudo-first order reaction with $[R^+] \ll [A]$, the differential equation can be solved by an exponential decay function (McEwan, 2015), and using theoretical knowledge of diffusion behaviour and gas and ion velocities in an electric field as well as experimental factors correcting for mass discrimination, one can estimate the analyte concentrations (Smith and Spanel, 2005). However, this is not very accurate for PTR-MS since it operates with a drift tube in which the ions are accelerated and guided via an electric field. Thus, the reagent ions are in excited state and ground-state kinetic constants are not valid anymore. Since SIFT-MS uses a flow tube that transports the ions through the gas flow, and only uses a small

voltage to minimize diffusion to the walls, near-thermal conditions apply and mixing ratios can be determined with an accuracy of ±35 % (Langford *et al.*, 2014).

Both instruments are comprised of the same three components: an ion generation zone, a reaction zone and a detection zone, cf. Fig. 1. Reagent ions H_3O^+ (both instruments), NO^+ and O_2^+ (SIFT-MS only, with positive ion source) are generated and

5   injected into the reaction zone, where they chemically ionize the analytes to form product ions, *e.g.* Eq. (R2) for methanol:

$$H_3O^+ + CH_3OH \rightarrow H_2O + CH_3OH_2^+ \tag{R2}$$

All ions are then analysed by a mass spectrometer (MS), usually a quadrupole-MS, separating the ions by their *m/z* ratio and then counting the number of ions hitting the multiplier.

There are two main differences between the two instruments: First, they differ in the way the reagent ions are generated and

10   second, whether the ions are reacting with the analyte in a drift-tube vs. in a flow-tube. Whereas PTR-MS uses hollow-cathode discharges to ionize water vapour generating H_3O^+ (Romano *et al.*, 2015), SIFT-MS generates a wet air plasma *via* microwave discharge and then selects the reagent ions H_3O^+, NO^+, and O_2^+ with a quadrupole (Smith and Spanel, 2005). Since the three reagent ions react differently with the analyte and may form different association and fragmentation products, more structural information can be obtained. However, the efficiency of creating the reagent ions is lower than for PTR-MS,

15   leading generally to higher limits of detection (LOD) for SIFT-MS.

PTR-MS uses a drift-tube, i.e. an evacuated tube on which an electric field is applied by several lenses that guides – focuses and accelerates – the ions through the reaction chamber toward the detector. This electric field accelerates and thus excites both reagent and product ions energetically. The SIFT-MS uses a flow tube with an inert carrier gas (He or N_2) that is mixed with the sample gas containing the analyte. Due to collisions with the carrier gas, in SIFT-MS the analytes and reagent ions

20   are approximately in thermal equilibrium. Because of their acceleration, the effective temperatures of the ions in the tube are much higher for PTR-MS than for SIFT-MS, and these differences in energy lead to different fragmentation patters for the two methods (Biasioli *et al.*, 2011). The carrier gas needed in SIFT-MS serves the additional role of reducing the amount of ion clustering, *e.g.* water clustering – formation of water adducts with ions, *e.g.* $H_3O^+ \cdot H_2O$ or $CH_3OH_2^+ \cdot H_2O$ – that can occur at high humidity.

25   To our knowledge there exists to date no systematic study that directly compares the two instruments under a range of humidity conditions. This can be important when measuring VOC emissions from plants or soils, where the humidity of the background air may vary with time, thereby potentially affecting the results. Direct comparisons of PTR-MS and SIFT-MS exist for breath analysis (Lourenço *et al.*, 2017; Smith *et al.*, 2014) and secondary organic aerosol formation (Li *et al.*, 2017), but neither study systematically investigates nor compares the effects of sample humidity on the results. For SIFT-MS,

30   humidity-dependence has been evaluated by Smith and Spanel (2000). Here, we present the missing piece: a systematic study based on calibrations at different humidities and low mixing ratios, evaluating the limit of detection, sensitivity and robustness for a Voice 200 ultra SIFT-MS (Syft Technologies, New Zealand) and a PTR-QMS 500 (Ionicon, Austria).

2   Experimental section

2.1   Materials

35   VOC-free air was generated by a Pure Air Generator (PAG 003, Ecophysics, Dürnten, Switzerland), and was further purified by a scrubber built into a Gas Calibration Unit (GCU, Ionicon, Austria). Gas mixtures of known VOC mixing ratios were produced by diluting a VOC standard gas mixture (Ionicon, Austria) (1 ppm each of 2-butanone, acetaldehyde, acetonitrile, acrolein, benzene, chlorobenzene, crotonaldehyde, dichlorobenzene, ethanol, isoprene, methanol, α-pinene, toluene, *o*-xylene in nitrogen). The GCU was used to dilute the standard to the mixing ratios used in the calibration. To minimize background,

40   the tubing used was 1/8" black PFA tubing with 1/8" Swagelok stainless steel connectors. Sample gas fluxes through the

multiport-inlet system were measured *via* a Sensidyne Gilian Gilibrator-2 NIOSH Primary Standard Air Flow Calibrator (Sensidyne, FL, USA).

2.2 SIFT-MS optimization

To improve the instrument background, several changes were applied to the Syft Voice 200 ultra with a positive ion source and a multi-port inlet. The shut-down valve in the carrier gas line was removed upon the advice of Marvin Shaw (University of York, GB). We also removed the vent valve for the backing pumps and just vent the system through the flow tube with purified air. All the Viton/FKM and nitrile o-rings delivered with the instrument were replaced by Hennlich FEP-coated FKM o-rings leading to a reduced background (see Fig. S2). Further, the VICI-valve that was delivered with the multi-port inlet system was switched to a flow-through VICI valve (EUT-6CSF16MWE) to allow continuous flushing of all lines to the ports and minimize dead volume, carry-over and the time the mixing ratio needs to stabilize.

Several inlet capillaries and a needle valve were tested for their contribution to overall instrument background. VICI silica-coated stainless steel capillaries with capillary sizes of 0.007", 0.010", and 0.015" inner diameter (ID) as well as PEEK capillaries (BOLA S1817-08, 0.25 mm ID, Bohlender, Germany, ChromaTec, 0.3 mm ID, Labomatic Instruments AG, Germany, PEEK Capillary Tubing 37010-20, 0.010" ID, Thermo Scientific, USA, and Latek Blue PEEK capillaries 8560 – 6009, 0.25 mm ID, Latek, Germany) as well as a Swagelok SS-SS2 needle valve were built into the multi-port inlet. For both dry and humid VOC-free air (90 % humidity at 25°C), a background was measured between m/z = 15 and 250 u (100 ms count time per ion, 10 scans). The background was normalized to both 10^6 counts of the respective reagent ion and the flowrate through the inlet capillary, see Fig. S1.

To ensure best performance, the microwave cavity and power, the upstream and downstream lenses, the source pressure and the air stream into the source were tuned before the measurements. Flow tube voltage and temperature, and carrier gas flow were optimized for VOCs with mixing ratios lower than 10 ppb. These experiments were performed using both helium and nitrogen as carrier gases, see Fig. S3-S14. Each time, 5 ppb of the VOC standard was mixed into dry and humid (90 % relative humidity at 25°C) VOC-free air. The flow tube voltage was scanned in 5 V steps between 0 and 65 V, the flow tube temperature was stepwise increased in 5°C intervals from 100 to 160°C, and the carrier gas flow was scanned at 0, 7.89, 15.79, 31.57, 47.36, 63.14, 78.93, 118.39, 157.85, 236.78, 315.71, 394.63, and 473.56 ccm (0-6 TorrL s^{-1}). For the scan, 15 scans were conducted with 500 ms dwell time – the time the detector integrates the signal – per ion after 20 s settle time.

To select for nitrogen versus helium as a carrier gas, calibrations were done in the range from 0.1 and 10 ppb for the VOC standard in dry air as well as at 30 %, 60 %, and 90 % relative humidity (25°C). For the measurement, after 20 s settle time, 15 scans were conducted with 500 ms dwell time per ion, except for α-pinene masses m/z = 81 and 137 u (H$_3$O$^+$ reagent ion), which were measured for 1 s, to account for its low mixing ratio due to its semivolatility in our soil samples.

2.3 Evaluation of different calibration procedures

The instrument calibration done with helium carrier gas (see Sect. 2.2) was used for evaluating different calibration procedures. As described in the methods section, different regression equations and calibration procedures were tested. In the following equations, I_P is the product ion intensity, I_R is the reagent ion intensity, χ is the mixing ratio of the analyte, ϕ is the relative humidity, ICF is the experimentally determined instrument calibration factor the SIFT-MS provides for correcting discrimination effects in flow tube and downstream quadrupole, k is the kinetic rate constant, $I_{H_3O^+}$ is the intensity of the H$_3$O$^+$ ion, $I_{H_3O^+ \cdot H_2O}$ the intensity of the H$_3$O$^+$·H$_2$O ion, and m, a, b, c, and d are regression parameters that are fitted. In the equations where more than one reagent and product ion was included (*e.g.* water clusters of product ions), the different ions were indexed by i and j.

Atmospheric
Measurement
Techniques
Discussions

1. Calibration for each humidity

    a. absolute product ion intensities: $I_P = m \cdot \chi_P + c$ (2)

    b. relative product ion intensities: $\frac{I_P}{I_R} = m \cdot \chi_P + c$ (3)

2. Calibration with linear humidity-dependence:

    a. Absolute product ion intensities: $\chi = m_1 \cdot I_P + m_2 \cdot \phi + b$ (4)

    b. Relative product ion intensities: $\chi = m_1 \cdot \frac{I_P}{I_R} + m_2 \cdot \frac{I_{H_3O^+}}{I_{H_3O^+ \cdot H_2O}} + b$ (5)

3. Based on the instrument's concentration result: $\chi_{substance} = \chi_{measured} \cdot \frac{k_1 \cdot I_{H_3O^+} + k_2 \cdot I_{H_3O^+ \cdot H_2O}}{c_1 \cdot k_1 \cdot I_{H_3O^+} + c_2 \cdot k_2 \cdot I_{H_3O^+ \cdot H_2O}}$ (6)

4. Calibration derived from physical parameters:

    a. Completely de novo: $\chi_{substance}(ppbv) = a \cdot \frac{I_{P_1^+} + \Sigma_{i=2}^{N}\left(b_i \cdot I_{P_i^+}\right)}{I_{R_1^+} + \Sigma_{j=2}^{M}\left(c_j \cdot I_{R_j^+}\right)} + d$ (7)

    b. Using the instrument calibration function: $\chi_{substance} = a \cdot \frac{\Sigma_i\left(I_{P_i^+} \cdot ICF_{P_i}\right)}{I_{R_1^+} \cdot ICF_{R_1} + \Sigma_j\left(b_j \cdot I_{R_j^+} \cdot ICF_{R_j}\right)} + c$ (8)

    c. De novo with relative values derived from Eq. (7): $\chi_{substance}(ppbv) = a \cdot \frac{\frac{I_{P_1^+}}{I_{R_1^+}} + \Sigma_{i=2}^{N}\left(b_i \cdot \frac{I_{P_i^+}}{I_{R_1^+}}\right)}{1 + \Sigma_{j=2}^{M}\left(c_j \cdot \frac{I_{R_j^+}}{I_{R_1^+}}\right)} + d$ (9)

From the raw data taken at each calibration point, the five datapoints before the last datapoint were used for the regression to minimize the effect of instable flows. Based on the blank measurement, the critical intensity was calculated by Eq. (10).

$$I_{crit} = \bar{I}_{Blank} + 3 \cdot sd(I_{Blank})$$ (10)

Only calibration points with means above the critical value were included in the regression. The evaluated ions are shown in Table S4. For the sake of simplicity, we will refer to the individual ions by *m/z*(reagent ion) / *m/z*(product ion) / analyte, *e.g.* 19 / 33 / methanol throughout the paper.

To assess the quality of the regression models, the Bayesian Information Criterion was calculated for each regression of the different compounds, see Eq. (11). Based on the variance of the residuals, it gives a measure of how well the model fits – a lower value shows a better fit of the model. In comparison to Akaike's Information Criterion, it punishes a higher number of parameters stronger (Veres, 1990).

$$BIC = n \log\left(\widehat{\sigma_R}^2\right) + k \log(n)$$ (11)

n… number of samples, $\widehat{\sigma_R}^2$… variance of the residuals, k … number of model parameters.

The BICs were calculated individually for each compound, but to get an overall idea on how the regression functions perform, mean, median, maximum and minimum of the BIC values of the compound obtained for each method were compared, see Table S5.

For the comparison of the SIFT-MS with the PTR-MS, each humidity was compared separately from the others following a basic calibration function, see Eq. (12).

$$\frac{I_{product\ ion}}{I_{reagent\ ion}} \cdot 10^6 = m \cdot [analyte] + c$$ (12)

The limit of detection (LOD) was estimated to be three times the standard deviation of the blank. The sensitivity was defined as the change in signal response by mixing ratio change, i.e. the slope of the respective calibration function. The confidence interval (CI) of the sensitivity was calculated as Eq. (13).

$$CI_{m,95\%} = t_{(p=95\%, df=26)} \cdot \frac{s_{yx}}{\sqrt{SS_{xx}}}$$ (13)

$t_{(p=95\%,df=26)}$ is the 95% value of Student's t-distribution for 26 degrees of freedom, $s_{y,x}$ the residual standard deviation, and $SS_{xx} = \sum_i (x_i - \bar{x})^2$ the sum of squares of the mixing ratios.

The signal to noise ratio was calculated by dividing the normalized product ion intensity at 1 ppb standard gas by the normalized product ion intensity of the blank (no VOC standard), Eq. (14).

$$SNR = \frac{I_{1ppb}}{I_{Blank}} \tag{14}$$

For the signal to noise ratio, upper and lower CIs were calculated separately, the upper CI by Eq. (15), the lower CI as Eq. (16), where $sd()$ is the standard deviation of the respective intensity.

$$CI^u_{SNR,95\%} = t_{p=95\%,df=7} \cdot \left(\frac{I_{1ppb}+sd(I_{1ppb})}{I_{Blank}-sd(I_{Blank})} - SNR \right) \tag{15}$$

$$CI^l_{SNR,95\%} = t_{p=95\%,df=7} \cdot \left(SNR - \frac{I_{1ppb}-sd(I_{1ppb})}{I_{Blank}+sd(I_{Blank})} \right) \tag{16}$$

2.4   Comparison of SIFT-MS and PTR-MS

The SIFT-MS was compared to a PTR-QMS 500 (Ionicon, Austria) by calibrating both instruments in the same manner as Sect. 2.3. For the calibrations, 10 measurements were performed at each mixing ratio for each level of humidity. For both instruments, the ion dwell time was set to 500 ms to ensure comparability. The α-pinene masses m/z = 81 and 137 u (H_3O^+ reagent ion) were measured for 1 s. The masses measured for the different compounds can be found in Table 1. The counts were normalized to 10^6 counts of the reagent ion. The PTR-MS was operated at E/N = 136 Td, and the counts of m/z = 19 u were inferred from its isotopic peak, m/z = 21 u.

2.5   SIFT-MS robustness over time

To test the SIFT-MS robustness over time, we did three calibrations as described in Sect. 2.3 for 60% humidity on one day (day 1) and repeated this one week later (day 8). All calibration curves were fitted with a linear regression. The significant difference of the slopes and intercepts of the two days was tested using an F-test (p = 95%, Bonferroni-corrected to 99.86%, n = 37) and depending on the result of the F-test, the homogeneous-variance or heterogeneous variance t-test (p = 95%, Bonferroni-corrected to 99.86%, for the correction n = 37) was applied. In addition to that, the 2 ppb calibration points from day 1 and day 8 were compared using a Bartlett test and an ANOVA (p = 95%, Bonferroni corrected to 99.935%, for the correction n = 77). Their relative standard deviation was calculated.

To evaluate a longer time scale, the workdaily measurement of a standard gas mixture of benzene, o-xylene, octafluorotoluene, hexafluorobenzene, ethylene, isobutane, tetrafluorobenzene, and toluene (2ppm each in nitrogen, Syft, New Zealand) was evaluated. A Neumann trend test was used to test for trends (p = 95%, n = 10).

To see the effect of venting the instrument on the calibrations, e.g. for maintenance or reparations, calibrations done in May 2018, December 2018, and January 2019, before and after the o-ring change and a detector shutdown, were conducted and compared as described above.

3   Results and discussion

Complete results of the different combinations of humidity conditions, carrier gas, flow tube temperature and voltage are given in the supplemental material; here we show selected comparisons under a subset of experiments and conditions that best illustrate the performance of the SIFT-MS and how it compares to the PTR-MS.

3.1 SIFT-MS-optimization to reduce background

Several changes were applied to the SIFT-MS to improve its limit of detection: The shut-down valve in the carrier gas line, and the vent valve for the backing pumps were removed, the inlet capillary was replaced by a needle valve (see Fig. S1) and all the original FKM and nitrile o-rings in the instrument were replaced with FEP-coated FKM o-rings (see Fig. S2). All

5   three measures led to a significant reduction of the instrument background, by up to factor 5 for some masses (see Fig. S2). In addition, the stop-flow VICI-valve of the multi-port inlet system was replaced by a flow-through VICI valve. This way, all lines to the ports can be flushed to minimize dead volume, carry-over and dwell time. In addition to the hardware changes, we also optimized a number of running parameters, including the flow tube voltage, flow tube temperature, carrier gas flow, and sample gas flow. The observed effects of water clustering, adduct formation, fragmentation and humidity-

10   sensitivity (see supplemental material) match the theoretical considerations of Smith and Spanel, 2005. Tests to optimize these parameters are described in detail in the supplemental material (see Fig. S3-S10). We also tested whether helium or nitrogen is a better carrier gas, both by optimizing the conditions (Fig. S11-S143) and a calibration (Table S1-S3). Nitrogen carrier gas lead to a higher sensitivity, but worse LODs and SNRs at 1 ppb and showed a higher humidity-sensitivity of the reagent ions, so we decided to use helium. Final running conditions for the SIFT-MS were: 40 V, 140°C, 158 ccm

15   (2 TorrL s^{-1}) Helium, and 100 sccm sample.

3.2 Humidity dependence of product ion intensities of the SIFT-MS

Humidity can have a big influence on the product ion intensity when H_3O^+ reagent ions are used: *e.g.* for α-pinene at 10 ppb, approx. one fourth of the intensity was lost, whereas the product ion intensity upon reaction with NO^+ or O_2^+ remains stable, see Fig. S15. Even for H_3O^+ ions, influences are mixed – for lower mass molecules like methanol (Fig. S16) and lower

20   mixing ratios (α-pinene, Fig. S15), the effect appears to be less prominent. For methanol, the intensity loss of m/z = 33 amu matches the intensity gain of m/z = 51 amu, the water cluster (Fig. S16). Both are ca. 50 cps for the humidity increase from 30 % to 90 %. However, for acetaldehyde, this is not the case – a loss of ca. 250 cps from 30 % to 90 % humidity is accompanied by a gain of ca. 50 cps of the water cluster (Fig. S17). This also does not match up if one assumes that the protonated product is the product of the reaction with H_3O^+ and the water cluster is the product of the reaction with $H_3O^+ \cdot$

25   H_2O – the reaction rate difference is rather insignificant (3.7·10^{-9} vs. 3.1·10^{-9} cm³ molecule^{-1} s^{-1}). For acetaldehyde, acetonitrile, and ethanol, the water cluster intensity rise does not match the intensity decline of the primary product ion, whereas for methanol and acrolein, it matches. Thus, high moisture sensitivity of the compound appears to correspond to this mismatch, whereas a low moisture sensitivity avoids it. In accordance with Wilson *et al.* (2003), we conclude that a back-reaction of the product ion with water might deionize the product ion to form a thermally colder reagent ion againand that

30   this might correspond to the proton affinity of the compound. Kebarle *et al.* (1976), published proton affinities of 187.3, 196.8, and 185.4, and 182.3 kcal mol^{-1} for acetaldehyde, ethanol, acetonitrile, and methanol. The difference was greatest for ethanol, having the highest proton affinity, and smallest for methanol. Only acrolein does not fit to this picture as it has a proton affinity of 190.4 kcal mol^{-1} (Del Bene, 1978), but this might be due to the different calculation used in the different paper.

35   In addition to that, we evaluated the effect when we normalize to the reagent ion counts. Fig. S18 and S19 show that whether the absolute signal is humidity sensitive or not, both show a linear humidity dependence after being normalized. For the lower toluene mixing ratios, this is not the case: in dry air the sensitivity is lower than for humid samples, but for the humidified samples, the trend is the same as for higher mixing ratios. This might be caused by problems with the bypass line of the humidifiers. For the humid calibrations at 30 –90 % relative humidity, this is not an issue and a linear humidity

40   dependence is observed here as well by normalizing to the reagent ion counts.

3.3 Evaluation of calibration procedures

To account for the humidity affecting the ion counts, several calibration procedures were tested. When using the chosen settings, the humidity has to be taken into account.

For the humidity sensitive ions, we first investigated whether the humidity is better represented by the actual relative

5   humidity or the ratio of the water cluster intensities, $\frac{I(H_3O^+\cdot H_2O)}{I(H_3O^+)}$. Since the ratio of the intensities correlates quite linearly with the relative humidity (Fig. S20) and is easy to measure *in situ*, the representation of the humidity as the intensity ratio appears to be more useful. Secondly, we tried normalizing to both $I(H_3O^+)$ and $I(H_3O^+) + I(H_3O^+ \cdot H_2O)$. Normalizing to both reagent ions makes the ion count more humidity dependent, but it also appears to make the humidity dependence more linear and decrease the variance in the data, (Fig. S21). Thus, we decided to normalize to both reagent ions. One has to keep

10   in mind though that this is only valid if they react with the analyte on a similar rate. If the kinetic rate constants are too different, the influence of the two reacting ions is not equal, so they should be treated differently. This is also why higher water clusters were not considered – they generally react roughly 1000 times slower.

Thirdly, to account for the humidity in the calibration, we tested the different methods described in the experimental section. Binning experimental results into humidity categories of 0 %, 30 %, 60 %, and 90 % as proposed in Eq. (2) and (3) is very

15   uncertain for humidities like 45% where both calibration curves are not very close. Assuming a linear humidity dependence as in Eq. (4) and (5) does not necessarily reflect the trends observed for lower mixing ratios, *e.g.* Fig. S19 where you can see a more curved shape. Additionally, a correction of the mixing ratio the instrument calculates was tested. This should be done carefully though since the results of all three reagent ions are averaged by the instrument if they do not differ too strongly, so one might actually induce error by correcting for humidity when the analyte is measured by multiple reagent ions. The most

20   exact version is calibration function Eq (7), which is derived from the function Syft uses to calculate mixing ratios based on the instrument parameters, Eq. (17):

$$\chi = k_B \cdot \frac{T_{FT}}{P_{FT}} \cdot \left(\frac{\varphi_{carr}}{\varphi_{samp}} + 1\right) \cdot \frac{\Sigma_{i=1}^N \left(I_{P_i} \cdot ICF_{P_i}\right)}{t_r \cdot br_i \cdot \Sigma_{j=1}^M \left(k_j \cdot I_{R_j} \cdot ICF_{R_j}\right)} \tag{17}$$

where k_B is the Boltzmann constant, T_{FT} is the flow tube temperature, P_{FT} the flow tube pressure, φ_{carr} and φ_{samp} the carrier gas and sample gas flows, I_{P_i} and I_{R_j} are product and reagent ion counts, ICF experimentally determined is the instrument

25   calibration factor accounting for ion discrimination of each ion, t_r is the reaction time, br_i the branching ratio of the ion, and k_j the rate constant of the reaction of the reagent ion with the analyte to form the product ion.

However, Eq. (8) quickly increases the number of parameters that need to be fitted: For example for methanol, the equation would be

$$\chi(ppbv) = a \cdot \frac{I(CH_3OH_2^+) + b \cdot I(CH_3OH_2^+ \cdot H_2O)}{I(H_3O^+) + c \cdot I(H_3O^+ \cdot H_2O)} + d \tag{18}$$

30   This is a four dimensional problem with four parameters. It cannot easily be plotted in two dimensions to see the quality of the fit, so one has to rely on the results of the fit without checking it visually. Using the ICFs determined during the validation reduces the number of fitted parameters, but still not the amount of dimensions. The most versatile method we found is Eq. (9), deriving from Eq. (7) by multiplying the fraction by $\frac{1}{I(H_3O^+)} / \frac{1}{I(H_3O^+)}$. This way, the equation is reduced by one dimension, so that if there are no product ion water clusters, one can visualize the results in a 3D plot, see Fig. 2. As

35   expected, the equation fits the data pretty well with a minimum of physically useful parameters and not relying on experimentally determined parameters other than the ion intensities.

To compare the models, the Bayesian Information Criterion (BIC) was calculated for the calibration of each substance by each method, cf. Table S5. Although the BIC punishes for a bigger number of parameters, still, Eq.s (7) and (9), the calibration functions based on actual theoretical considerations, consistently have the smallest BIC and thus fit the data best.

40   This fits the considerations above. Thus, for humidity dependent ions, this is the method of choice.

However, since to the knowledge of the authors parameters that access the quality of a calibration like LOD, sensitivity, SNR, precision and robustness are only established for a 2D calibration curve, for the following comparison with the PTR-MS, we used the simple humidity independent regression based on normalized ion counts, Eq. (3). This is the most accessible and the easiest to compare with PTR-MS, especially because the humidity is known and does not need to be

5   compared by $I(H_3O^+ \cdot H_2O) \, / \, I(H_3O^+)$.

3.4   Comparison of SIFT-MS to PTR-MS

The optimized SIFT-MS was compared to the PTR-MS using the diluted Ionicon calibration standard (mixing rations between 0.25 and 10 ppb), and for each mixing ratio at 10 %, 30 %, 60 %, and 90 % relative humidity (25°C). Although we evaluated different methods for calibrating the instrument with one calibration function (see above), we directly compared

10   the separate calibrations of PTR-MS and SIFT-MS done for each humidity, *e.g.* the PTR-MS calibration at 30 % humidity vs. the SIFT-MS calibration at the same humidity. In the graphs, the results for 30 % humidity are shown, and the results for all humidities are summarized in Table S6–S11.

At all humidities, the limit of detection (LOD) was lower for PTR-MS. While the LOD of PTR-MS is between 10 and 100 ppt for most masses, the LODs of the SIFT-MS are generally one order of magnitude higher, between 100 ppt and

15   1 ppb, see Fig. 3 and Table S6–S7. This is probably due to three factors: First, the flow into the PTR-MS is about three times as high, so that more analyte is ionized. Second, the reagent ion counts (*e.g.* H$_3$O$^+$) are twice as high for the PTR-MS, doubling the number of product ions, thus more are detected. This was also discussed by Smith, D. *et al.* (2014), who also report lower LODs for PTR-MS in their review. Third, the variation in the signal over time is much lower for PTR-MS, maybe due to more stable conditions in the flow tube. This can also be inferred from the calibration curves of Lourenço, C.

20   *et al.* (2017), as their R² value is lower for SIFT-MS than for PTR-MS. However, the difference in LOD between the instruments is smaller than was previously found: Blake *et al.* (2009) estimated a difference of two orders of magnitude whereas we found only one order of magnitude. On the other hand, Milligan *et al.* (2007) presented a SIFT-MS with LODs in the mid-ppt-range, so very low values are possible on custom-built instruments. Thus, instrument improvements by Syft over the last 10 years as well as our improvements to the SIFT-MS instrument significantly improved LOD.

25   The upper limit of the dynamic range is not limited by the detector since for count rates saturating the detector (around $2 \cdot 10^6$ counts), the dwell time can be shortened. This of course leads to lower precision, but one can still obtain results. The upper limit of the dynamic range is determined by the amount of reagent ion which should be at least in 10x higher abundance than the product ion counts – for calculating the mixing ratio, it is assumed that the reagent ion counts are do not change upon reaction (Smith and Spanel, 2005). Thus, product ion counts of more than 10^6 cps for PTR-MS and $5 \cdot 10^5$ cps for SIFT-MS

30   should not be reached. This equates to low ppm levels, so both instruments have a dynamic range of five orders of magnitude with the dynamic range of the SIFT-MS being a bit smaller than the one of PTR-MS.

For the sensitivity analysis, the slopes of the calibration curve based on ion intensities normalized to 10^6 reagent ions were compared. In general, the SIFT-MS is more sensitive, and appears to become even more sensitive the higher the *m/z* ratio becomes: For methanol, both instruments are comparable, for toluene, the sensitivity is at least twice as high, see Fig. 4 and

35   Table S8–S9. These results are different from the results of Lourenço, C. *et al.* (2017), where PTR-MS shows a higher sensitivity by a factor of 10, but match the reports of Prince *et al.* (2010) for SIFT-MS sensitivity. Still, due to a higher precision of the PTR-MS data that is also reflected in the much lower LOD, the signal to noise ratio at 1 ppb is still much higher for the PTR-MS than for the SIFT-MS.

This also influences the signal to noise ratios, see Fig. 5 and Table S10–11. For smaller masses, the PTR-MS has a much

40   higher SNR, whereas for the higher masses of the aromatic molecules like dichlorobenzene, *o*-xylene and toluene, the SIFT-MS has a higher SNR. With these molecules, the PTR-MS has a comparable LOD and a lower sensitivity, so this adds up to a lower SNR.

To compare instrument robustness, defined here as changes in signal intensity over time or with varying conditions, one has to consider two factors: (i) robustness against moisture and (ii) robustness over time. We observed that PTR-MS tends to be less robust against humidity. As the example for α-pinene in Fig. 4 shows, PTR-MS has an optimum at low humidity whereas the SIFT-MS with H_3O^+ and O_2^+ shows a rather stable signal. However, one has to note that this has to be tested for

5   each compound product ion separately, as the humidity dependence of α-pinene upon reaction with NO^+ illustrates. Humidity affects the sensitivity to a greater extent than the LOD, so especially for PTR-MS, a calibration in the targeted humidity-range or calibrating also for humidity using Eq. (9) is advisable.

For the robustness over time, we unfortunately cannot provide information for the PTR-MS as we used it only for this study. For the SIFT-MS, we did three calibrations at 60% humidity on one day (day 1), and repeated this one week later (day 8).

10   Standard calibration curves for α-pinene are shown in Fig. 8. We compared the two days by doing F- and t-tests on the slopes and the intercepts of the calibration curves, separately for each reagent ion. The slopes were not heteroscedastic and the difference between the two days was not statistically significant (p = 95%), whereas the F-tests failed for the intercepts, but the heterogeneous variance t-tests on the intercepts again did not show statistically significant differences between the intercepts of day 1 and day 8 (p = 95%). Additionally, we tested the variance in signal intensity of the 2 ppb calibration

15   point. Here, we included the two interacting factors to which day and to which calibration the raw data measurements belong. The Bartlett tests did not show heteroscedasticity, and the two-way ANOVA with the two interacting factors day and number of calibration only showed significant difference of the day for the ion 19 / 75 / acrolein / $C_3H_5O^+ \cdot H_2O$, i.e. the water cluster of acrolein. Maybe the air humidity of the produced calibration standard varied enough to make it statistically significant. Thus, over the course of a week, the calibrations appear to be stable and can be used to calculate mixing ratios.

20   We are not aware of a similar study published, however, Ammann *et al*. (2004) showed loss of detector signal intensity over a period of two months during their field experiment with PTR-MS. When comparing the signal intensity measured during weekly validation of the instrument, we observe the same trend, Fig. S23. A Neumann trend test was negative for the ions (p = 95%, n = 10), but the signal appears to be dropping. The trends might become significant however over a longer time period. Combining those two experiments, we conclude that the calibration is stable over the course of days to weeks.

25   In addition to that, we compared the calibrations that we did in May, December and January, done after the o-ring change and a detector crash. Considerable variation in LOD and sensitivity we observed (Fig. S22) indicates that a regular calibration should be conducted, especially after repairing or doing maintenance on the instrument. Syft tackles this problem by providing a daily automated validation procedure, but this only validates at 2 ppm of the standard substances in dry air. We adjusted the procedure to our low mixing ratio regime by diluting the standard to 20 ppb for validation. For routine

30   measurements of a rather stable system with rather high mixing ratios (above ppb level), *e.g.* clean room air quality monitoring, this should be enough, but for accurate quantification of dilute analytes in a varying system with different humidities, for example our soil VOC emission monitoring during dryout-incubations from flooded to dry soil, we recommend calibrating the instrument before every experiment series versus the multiple standard gas and validate daily with the adapted Syft routine.

35   **4   Conclusions**

The comparison of SIFT-MS and PTR-MS confirmed that PTR-MS has a lower LOD than SIFT-MS, though modification of the SIFT-MS instrument improved its LOD to within an order of magnitude of the PTR-MS. Both instruments are equally sensitive responding to signal changes and have similar dynamic range. The calibration at multiple humidities demonstrated that PTR-MS is more humidity dependent than SIFT-MS, indicating that it is important to calibrate for the humidity as well,

40   or take care that it remains constant during measurements. The SIFT-MS is stable over shorter time periods, as we could demonstrate by comparing calibrations a week apart that are not significantly different. However, it shows considerable

variations in signal intensity over longer periods, so that at least after each maintenance, the instrument should be calibrated: the LOD varied by up to a factor of two, the sensitivity by up to a factor of three. This drawback was addressed by Syft by implementing a workdaily validation routine that takes approx. 10 min that we adjusted to work for low mixing ratios, so the instrument calibration factor balancing out the mass discrimination should account for those instabilities. Still, we calibrate our instrument with humidity before every experiment series in addition to the one-point validation of the SIFT-MS procedure. Plus, the additional structural information that can be gained by SIFT-MS is helpful especially for more complex mixtures. Thus, PTR-MS is better suited for dry air studies of simple gas mixtures of well-known composition and when working with dilute samples. SIFT-MS is better suited for studies in humid air or under changing humidity conditions as well as for more complex mixtures of unknown composition like our soil emission monitoring during dryout incubation experiments.

5   Code and data availability

Code and data are published as Lehnert, A.-S., Behrendt, T., Ruecker, A., Pohnert, G., Trumbore, S. E.: Max Planck Society, https://dx.doi.org/10.17617/3.2u, 2019.

6   Author contribution

The study was designed by A.S.L., T.B. and G.P. Experiments were performed by A.S.L. with assistance from T.B. and A.R. Data processing and analysis was done by A.S.L. with assistance from T.B. and A.R. Manuscript was written by A.S.L. All authors assisted with data interpretation, discussion of results and helped to improve the quality of the manuscript.

7   Competing interests

The authors declare that they have no conflict of interest.

8   Acknowledgements

9   References

Amelynck, C., Schoon, N., and Dhooghe, F.: SIFT Ion Chemistry Studies Underpinning the Measurement of Volatile Organic Compound Emissions by Vegetation, Curr. Anal. Chem., 9, 540-549, https://dx.doi.org/10.2174/15734110113099990018, 2013.

Ammann, C., Spirig, C., Neftel, A., Steinbacher, M., Komenda, M., and Schaub, A.: Application of PTR-MS for measurements of biogenic VOC in a deciduous forest, Int. J. Mass Spectrom., 239, 87-101, https://dx.doi.org/10.1016/j.ijms.2004.08.012, 2004.

Biasioli, F., Yeretzian, C., Märk, T. D., Dewulf, J., and Van Langenhove, H.: Direct-injection mass spectrometry adds the time dimension to (B)VOC analysis, Trends Anal. Chem., 30, 1003-1017, https://dx.doi.org/10.1016/j.trac.2011.04.005, 2011.

Blake, R. S., Monks, P. S., and Ellis, A. M.: Proton-Transfer Reaction Mass Spectrometry, Chem. Rev., 109, 861-896,
5   https://dx.doi.org/10.1021/cr800364q, 2009.

Bylinski, H., Gebicki, J., Dymerski, T., and Namiesnik, J.: Direct Analysis of Samples of Various Origin and Composition Using Specific Types of Mass Spectrometry, Crit. Rev. Anal. Chem., 47, 340-358, https://dx.doi.org/ 10.1080/10408347.2017.1298986, 2017.

Casas-Ferreira, A. M., Nogal-Sanchez, M. D., Perez-Pavon, J. L., and Moreno-Cordero, B.: Non-separative mass
10   spectrometry methods for non-invasive medical diagnostics based on volatile organic compounds: A review, Anal. Chim. Acta, 1045, 10-22, https://dx.doi.org/ 10.1016/j.aca.2018.07.005, 2019.

Davis, B. M. and McEwan, M. J.: Determination of Olive Oil Oxidative Status by Selected Ion Flow Tube Mass Spectrometry, J. Agricult. Food Chem., 55, 3334-3338, https://dx.doi.org/10.1021/cr800364q, 2003.

Davis, B. M., Senthilmohan, S. T., Wilson, P. F., and McEwan, M. J.: Major volatile compounds in head-space above olive
15   oil analysed by selected ion flow tube mass spectrometry, Rapid Commun. Mass Spectrom., 19, 2272-2278, https://dx.doi.org/10.1002/rcm.2056, 2005.

Del Bene, J. E.: A molecular orbital study of protonation. 3. Equilibrium structures and energies of ions RCHOH, J. Am. Chem. Soc., 100, 1673-1679, https://dx.doi.org/10.1021/ja00474a006, 1978.

Herrington, J. S.: Ambient Air Sampling with Whole-Air, In-Field Concentration and Particulate Matter (PM)
20   Methodologies, in: Comprehensive Analytical Chemistry, edited by: Forbes, P. B. C., Elsevier, 109-153, https://doi.org/10.1016/bs.coac.2015.09.004, 2015.

Jordan, A., Haidacher, S., Hanel, G., Hartungen, E., Herbig, J., Märk, L., Schottkowsky, R., Seehauser, H., Sulzer, P., and Märk, T. D.: An online ultra-high sensitivity Proton-transfer-reaction mass-spectrometer combined with switchable reagent ion capability (PTR+SRI−MS), Int. J. Mass Spectrom., 286, 32-38, https://dx.doi.org/10.1016/j.ijms.2009.06.006, 2009.

25   Kebarle, P., Yamdagni, R., Hiraoka, K., and McMahon, T. B.: Ion molecule reactions at high pressure: recent proton affinities, gas phase acidities and hydrocarbon clustering results, Int. J. Mass Spectrom. Ion Phys., 19, 71-87, https://doi.org/10.1016/0020-7381(76)83005-7, 1976.

Langford, V. S., Graves, I., and McEwan, M. J.: Rapid monitoring of volatile organic compounds: a comparison between gas chromatography/mass spectrometry and selected ion flow tube mass spectrometry, Rapid Commun. Mass Spectrom., 28, 10-
30   18, https://dx.doi.org/10.1002/rcm.6747, 2014.

Li, L., Qi, L., and Cocker, D. R.: Contribution of methyl group to secondary organic aerosol formation from aromatic hydrocarbon photooxidation, Atmos. Environ., 151, 133-139, https://dx.doi.org/10.1016/j.atmosenv.2016.11.064, 2017.

Lourenço, C., González-Méndez, R., Reich, F., Mason, N., and Turner, C.: A potential method for comparing instrumental analysis of volatile organic compounds using standards calibrated for the gas phase, Int. J. Mass Spectrom., 419, 1-10,
35   https://dx.doi.org/10.1016/j.ijms.2017.05.011, 2017.

McEwan, M. J.: Direct Analysis Mass Spectrometry. In: Ion/Molecule Attachment Reactions: Mass Spectrometry, edited by Fujii, T., Springer, Boston, USA, 263-317, https//dx.doi.org/ 10.1007/978-1-4899-7588-1_8, 2015.

Milligan, D. P., Wilson, P. F., Mautner, M. N., Freeman, C. G., McEwan, M. J., Clough, T. J., and Sherlock, R. R.: Atmospheric Pollutants and Trace Gases, J. Environ. Qual., 31, 515, https://dx.doi.org/10.2134/jeq2002.5150, 2002.

40   Milligan, D. P., Francis, G. J., Price, B. P., and McEwan, M. J.: Demonstration of Selected Ion Flow Tube MS Detection in the Parts per Trillion Range, Anal. Chem., 79, 2537-2540, https://doi.org/10.1021/ac0622678, 2007.

Pienaar, J. J., Beukes, J. P., Van Zyl, P. G., Lehmann, C. M. B., and Aherne, J.: Passive Diffusion Sampling Devices for Monitoring Ambient Air Concentrations, in: Comprehensive Analytical Chemistry, edited by: Forbes, P. B. C. , Elsevier, 13-52, https://doi.org/10.1016/bs.coac.2015.09.002, 2015.

5   Prince, B. J., Milligan, D. B., and McEwan, M. J.: Application of selected ion flow tube mass spectrometry to real-time atmospheric monitoring, Rapid Commun. Mass Spectrom., 24, 1763-1769, https://dx.doi.org/ 10.1002/rcm.4574, 2010.

Romano, A., Capozzi, V., Spano, G., and Biasioli, F.: Proton transfer reaction-mass spectrometry: online and rapid determination of volatile organic compounds of microbial origin, Appl. Microbiol. Biotechnol., 99, 3787-3795, https://dx.doi.org/10.1007/s00253-015-6528-y, 2015.

Schwarz, K., Filipiak, W., and Amann, A.: Determining concentration patterns of volatile compounds in exhaled breath by
10   PTR-MS, J. Breath Res., 3, 027002, https://dx.doi.org/10.1088/1752-7155/3/2/027002, 2009.

Shende, P., Vaidya, J., Kulkarni, Y. A., and Gaud, R. S.: Systematic approaches for biodiagnostics using exhaled air, J. Controlled Release, 268, 282-295, https://dx.doi.org/10.1016/j.jconrel.2017.10.035, 2017.

Spanel, P. and Smith, D.: Influence of water vapour on selected ion flow tube mass spectrometric analyses of trace gases in humid air and breath, Rapid Commun. Mass Spectrom., 14, 1898-1906, https://doi.org/ 10.1002/1097-
15   0231(20001030)14:20<1898::AID-RCM110>3.0.CO;2-G, 2000.

Smith, D. and Spanel, P.: Selected ion flow tube mass spectrometry (SIFT-MS) for on-line trace gas analysis, Mass Spectrom. Rev., 24, 661-700, https://dx.doi.org/10.1002/mas.20033, 2005.

Smith, D. and Spanel, P.: Direct, rapid quantitative analyses of BVOCs using SIFT-MS and PTRMS obviating sample collection, Trends Anal. Chem., 30, 945-959, https://dx.doi.org/10.1016/j.trac.2011.05.001, 2011.

20   Smith, D., Spanel, P., Herbig, J., and Beauchamp, J.: Mass spectrometry for real-time quantitative breath analysis, J. Breath Res., 8, 027101, https://dx.doi.org/10.1088/1752-7155/8/2/027101, 2014.

Spanel, P., Spesyvyi, A., and Smith, D.: Electrostatic switching and selection of H_3O^+, NO^+ and O_2^{+*} reagent ions for selected ion flow-drift tube mass spectrometric analyses of air and breath, Anal. Chem., https://dx.doi.org/10.1021/acs.analchem.9b00530, 2019.

25   Veres, S. M.: Relations between information criteria for model-structure selection Part 1. The role of bayesian model order estimation, Int. J. Control, 52, 389-408, https://dx.doi.org/10.5194/bgd-11-12009-2014, 1990.

Wilson, P. F., Freeman, C. G., and McEwan, M. J.: Reactions of small hydrocarbons with H3O+, O2+ and NO+ ions, Int. J. Mass spectrom., 229, 143-149, https://dx.doi.org/10.1016/s1387-3806(03)00290-2, 2003.

Yuan, B., Koss, A. R., Warneke, C., Coggon, M., Sekimoto, K., and de Gouw, J. A.: Proton-Transfer-Reaction Mass
30   Spectrometry: Applications in Atmospheric Sciences, Chem. Rev., 117, 13187-13229, https://dx.doi.org/10.1021/acs.chemrev.7b00325, 2017.
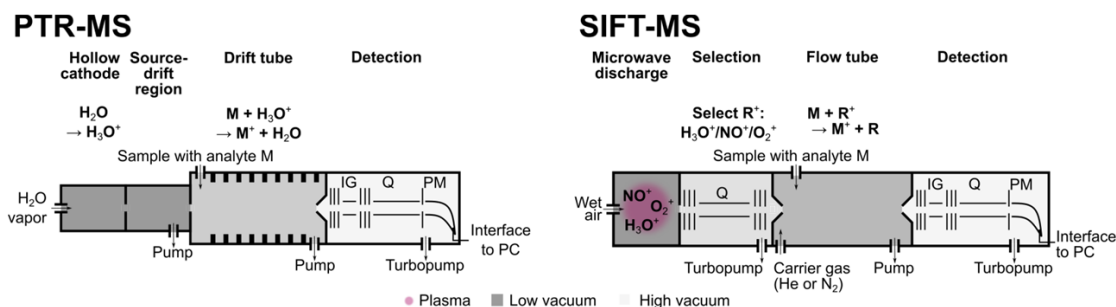
Figure 1: Schemes of PTR-MS and SIFT-MS instrument components. PTR-MS ionizes water vapor in a hollow-cathode. The analyte is
35   injected into the flow tube, where it reacts with the H_3O^+ reagent ion and is accelerated in the electric field. The ions are detected *via* a quadrupole mass spectrometer consisting of an ion guide (IG), a quadrupole (Q) and a particle multiplier (PM). SIFT-MS generates a plasma from wet air and then selects the reagent ion R (H_3O^+, NO^+ or O_2^+) via a quadrupole (Q). In the flow tube, reagent ions R^+ and

analytes M meet and react. Their reaction time is defined by the flow of the carrier gas through the tube and a small electric field to focus the ions. Like in PTR-MS, the ions are detected *via* a quadrupole-MS.
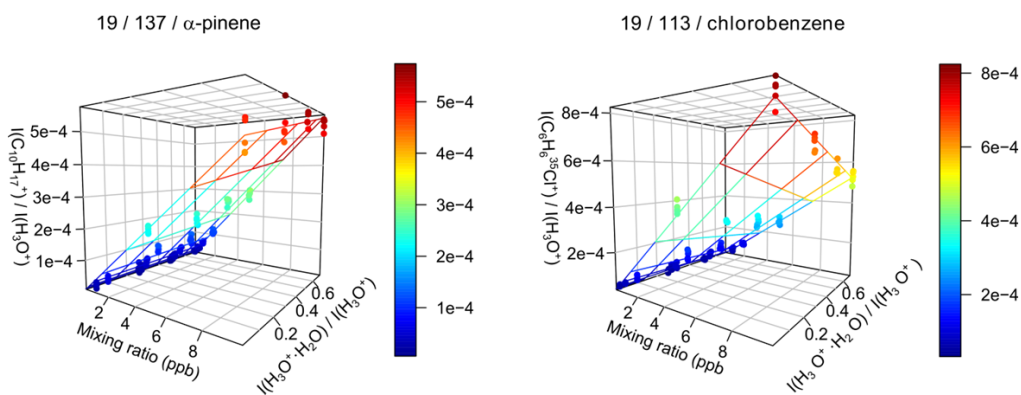
5   **Figure 2:** Relative product ion intensities and calibration plane for α-pinene and chlorobenzene using Eq. (9). Even strong humidity-dependence like for chlorobenzene is accounted for using this method. $I(C_{10}H_{17}^+)/I(H_3O^+)$ and $I(C_6H_6^{35}Cl^+)/I(H_3O^+)$ are the relative product ion intensities of the two mentioned ions, $I(H_3O^+ \cdot H_2O)/I(H_3O^+)$ serves as measure for the humidity.
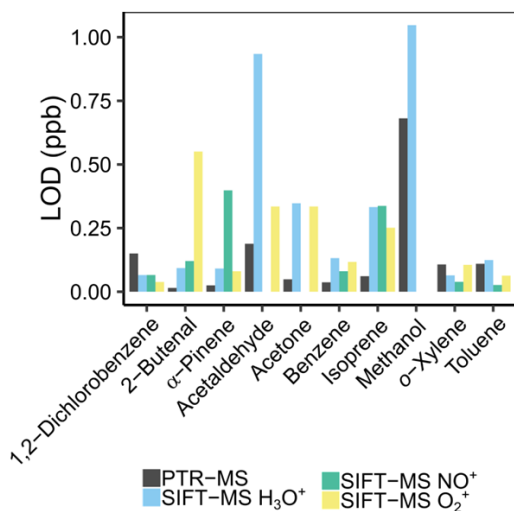
    Figure 3: Comparison of the limit of detection (LOD) for PTR-MS and the different reagent ions of the SIFT-MS of the shown VOCs at
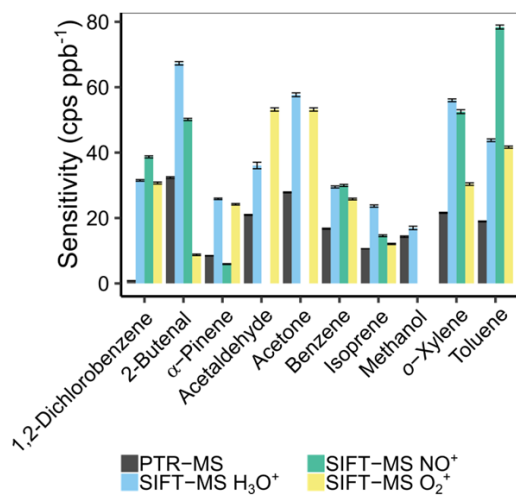10   30 % humidity.

Figure 4: Instrument sensitivity ± 95 % confidence interval (df = 26) of PTR-MS and the different SIFT-MS reagent ions for different VOCs at 30 % humidity. Sensitivity is defined here as the slope of the calibration curve.
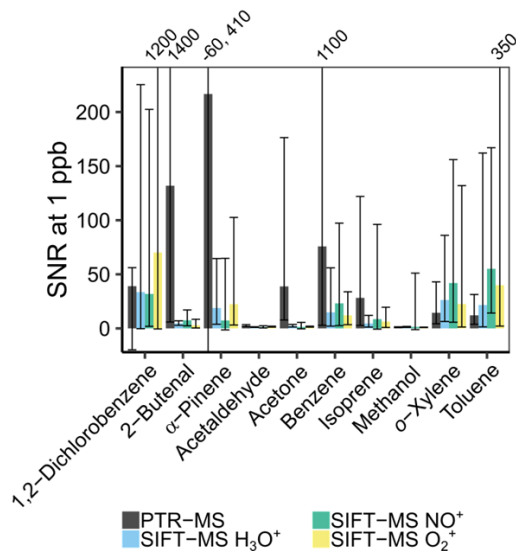

5   **Figure 5:** Signal to noise ratio (SNR) at 1 ppb (± 95 % CI, df = 7) of PTR-MS and the different SIFT-MS reagent ions for different VOCs at 30 % humidity. The values above the biggest error bars resemble the values of the confidence intervals out of the depicted range. The high positive confidence interval is due to the high relative error of the blank.
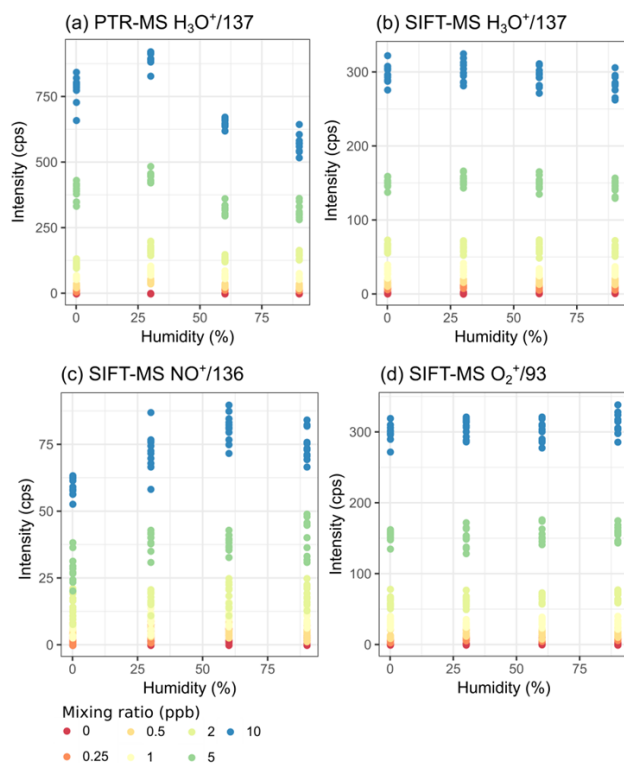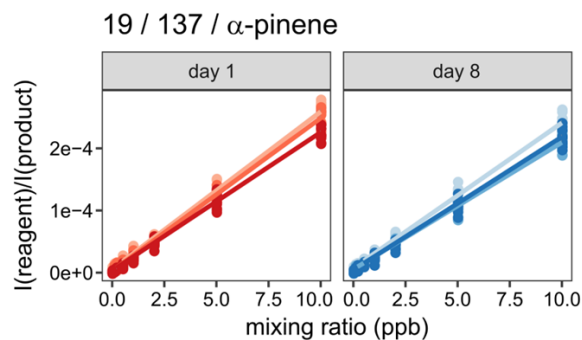
Figure 6: Humidity-dependence as a change in signal intensity with humidity for mixing ratios between 0.25 and 10 ppb of the α-pinene signal for PTR-MS (a) and the different SIFT-MS reagent ions (b–d) with their most abundant product ion.

Figure 7: Robustness of the α-pinene calibration of the SIFT-MS. Three calibrations were conducted on one day, and one week later, on day 8. Slopes and intercepts were not significantly different (p = 0.9986, n = 3) between the days.

Atmospheric
Measurement
Techniques
Discussions

Table 1: Measured ions (m/z in u) for SIFT-MS and PTR-MS to compare the compounds of the VOC standard.

substance	m/z(SIFT-MS) in u			m/z(PTR-MS) in u
	H_3O^+	NO^+	O_2^+	
α-pinene	81, 137, 155	136	93	81, 137
1,4-dichlorobenzene	147	146	146	148
2-butenal	71, 89	69	69, 70	71
acetaldehyde	45, 63	43	43	45
acetone	59, 77	88	43, 58	59
acetonitrile	42, 60	71	-	42
acrolein	57, 75	55, 86	28, 55	75
benzene	79	78, 108	78	79